Identification of a key oncogenic role of p63 in altered-FGFR3 tumors through inference of bladder cancer gene regulatory network and functional validations

Aura Ileana Moreno Vega, Macarena Zambrano, Julia Puig, Florent Dufour, Clarice Groeneveld, Mingjun Shi, Claire Beraud, Myriam Lasalle, Elodie Chapeaublanc, Thierry Lebret, et al.

▶ **To cite this version:**

Aura Ileana Moreno Vega, Macarena Zambrano, Julia Puig, Florent Dufour, Clarice Groeneveld, et al.. Identification of a key oncogenic role of p63 in altered-FGFR3 tumors through inference of bladder cancer gene regulatory network and functional validations. 2023. hal-04687147

HAL Id: hal-04687147
https://hal.science/hal-04687147v1

Preprint submitted on 4 Sep 2024

HAL is a multi-disciplinary open access archive for the deposit and dissemination of scientific research documents, whether they are published or not. The documents may come from teaching and research institutions in France or abroad, or from public or private research centers.

L'archive ouverte pluridisciplinaire **HAL**, est destinée au dépôt et à la diffusion de documents scientifiques de niveau recherche, publiés ou non, émanant des établissements d'enseignement et de recherche français ou étrangers, des laboratoires publics ou privés.

Identification of a key oncogenic role of p63 in altered-FGFR3 tumors through inference of bladder cancer gene regulatory network and functional validations.

Aura Moreno-Vega[1*], Macarena Zambrano[2*], Julia Puig[3*], Florent Dufour[1], Clarice Groeneveld[1,4], Mingjun Shi[1], Claire Beraud[5], Myriam Lasalle[5], Elodie Chapeaublanc[1], Thierry Lebret[6], Philipe LLuel[5] , Ana Maria Eijan[2], Lars Dyrskjot[7], Mohamed Elati[3,#], François Radvanyi[1,#], Catalina Lodillinsky[2,#] and Isabelle Bernard-Pierrot[1,#,@]

---

[1] Institut Curie, CNRS, UMR144, Molecular Oncology team, PSL Research University, Paris, France; b Paris-Sud University, Paris-Saclay University, Paris, France;

[2] Research Area, Institute of Oncology Angel H. Roffo, University of Buenos Aires, Buenos Aires, Argentina

[3] Univ. Lille, CNRS, Inserm, CHU Lille, UMR9020 – UMR-1277 - Canther, F-59000 Lille, France

4 La ligue contre le cancer, Paris, France

[5] Urosphere, Toulouse, France

[6] Service d'Urologie, Hôpital Foch, Suresnes, France

[7] Department of Molecular Medicine, Aarhus University Hospital, Aarhus, Denmark

In preparation for submission

* These authors contributed equally to the work

# These authors co-supervised the study

@ To whom correspondence should be addressed.

Dr Isabelle Bernard-Pierrot

Institut Curie

12 rue Lhomond

75005 Paris

E-mail: isabelle.bernard-pierrot@curie.fr

Tel: +33 1 42 34 63 40, Fax: +33 1 42 34 63 49

Abstract

The alteration of the receptor tyrosine kinase FGFR3 through activating mutations or translocations is one of the most common genetic events in bladder cancer (BLCA). Despite the demonstration of the oncogenic potential of such alterations, the gene regulatory network of an altered-FGFR3 in bladder cancer remains poorly characterized. We combined here a bioinformatic reverse-engineering inference approach together with *in vitro* and *in vivo* FGFR3-perturbation experiments to determine a BLCA regulatory network of transcription factors and co-factors (TFs/coTFs) that are driven by an altered-FGFR3 and critical for its oncogenic activity. Amongst them, we identified p63 in both non-muscle (NMIBC) and muscle invasive bladder cancers (MIBC) and further demonstrated that it mediates tumor growth, cell proliferation and migration of FGFR3-dependent bladder cancer cells. In Ta NMIBC, we observed both higher p63 activity and increased tendency of recurrence in tumors harboring a mutated-FGFR3 as compared to tumors with the wild-type receptor, suggesting that p63 activation by FGFR3 could favor recurrence. Our results elucidate an unexpected oncogenic key role of p63 in luminal papillary tumors bearing FGFR3 mutations and provide a global BLCA specific FGFR3-induced gene regulatory network that should allow a better understanding of FGFR3 induced oncogenic dependency that could have clinical applications.

Introduction

Bladder cancer is the fourth most common cancer in men in industrialized countries and it can be divided into two main groups based on tumor stage. Non-muscle invasive bladder carcinoma is the most frequent subtype at first diagnosis (NMIBC, 75% of patients) and although it is of good prognosis (80% five-year survival rate), an important percentage of patients recur following initial treatment (70% of patients). Furthermore, depending on grade and stage, 5-75% of NMIBC patients will progress into muscle-invasive disease (MIBC) [1,2]. Contrary to NMIBC, MIBC is a life-threatening disease with a five-year survival of less than 60%, which decreases to less than 6% in presence of metastasis[3,4].

The treatment of bladder cancer remains challenging and very expensive due to two different clinical problems: (1) the high recurrence of NMIBC leading to a costly long-term follow-up and (2) the poor survival rate of MIBC, a disease for which there are almost no efficient treatments available. Recently, promising results have been reported in clinical trials targeting FGFR3, a frequently altered receptor tyrosine kinase (RTK) in bladder cancer[5–8]. Activating mutations affecting *FGFR3* are amidst the most commonly observed genetic alterations in bladder cancer, being present in more than 65% of NMIBCs (enriched in Class 1 and Class 3 subtypes) and 15% of MIBCs (enriched in luminal papillary subtype)[9,10]. Moreover, translocations leading to active *FGFR3* gene fusions can be observed in 3% of

MIBCs and 30% of MIBCs that present a wild-type *FGFR3*, overexpress the receptor[11–13]. In 2019, the FDA approved the first pan-inhibitor directed against FGFRs in advanced bladder cancer. However, as previously reported in preclinical bladder cancer models and in other targeted therapies in different cancer types (EGFR, BRAF, KIT; lung cancer, melanoma, gastrointestinal stromal tumors), patients are expected to develop resistance to RTK-targeting treatment[14–19]. As the FGFR3 gene regulatory network in bladder cancer remains poorly characterized, a deeper understanding of such network would allow to better comprehend the role of the receptor in the disease and identify new therapeutic targets. Most importantly, the identification of novel targets would improve existing FGFR3-targeting therapies and/or prevent the development of resistance to treatment. The identification of MYC; of one key TF activated by FGFR3, already allowed us to propose optional therapeutic strategies by inhibiting the FGFR3-MYC regulatory loop[20]. One of the main aims of this study is to provide a global FGFR3 regulatory network that may be used in the future to discover new driver regulators of therapeutic interest.

There exist many different bioinformatic methods to infer gene regulatory networks (GRNs) from high-throughput data, enabling the discovery of disease-driver genes and or pathways. Up to date, among the approaches that have proved successful are those that allow for the reverse-engineered construction of context-specific networks (e.g. ARACNe, LICORN, GENIE3) and which can be further enriched through the integration of interaction evidences (protein-protein interactions and/or transcriptional regulation)[21–25]. Here, we use the hybrid-learning co-operative regulation networks (H-LICORN) algorithm that integrates data-mining methods with numerical linear regression to efficiently infer a context-specific GRN[26,27]. More specifically, we predicted a cooperativity network of transcription factors and cofactors (TFs/coTFs; co-activators and co-repressors) using transcriptomic data from FGFR3-mutated bladder cancer cell lines and human bladder tumors. Employing experimentally derived data where the expression or activity of FGFR3 was altered in *in vitro* and *in vivo* preclinical models, we highlighted the TFs and coTFs from the network that are driven by an altered FGFR3. Additionally, we identified the essential regulators of such network through the use of publicly available cell viability data from large CRISPR-Cas9-based screen in FGFR3-dependent bladder cancer cell lines[28]. An important result from our study was the identification of p63 as an essential and active transcription factor forming part of the FGFR3-driven regulatory network in bladder cancer. We further showed, that it regulates tumor growth, cell proliferation, migration and invasion through extra-cellular matrix degradation. These functional findings are relevant as they may help to better understand certain phenotypes that are present in FGFR3-dependent tumors, such as the one we discuss in this study: a higher tendency of recurrence observed in FGFR3-mutated tumors that could be associated with a higher P63 activity.

Results

Bladder-cancer gene regulatory network of TFs and coTFs in FGFR3-altered tumors.

Using the CoRegNet package (Bioconductor), we generated a GRN from the transcriptome of the 36 bladder cancer cell lines of the CCLE 2019Q1 and refined it via the integration of protein-protein interactions (ppis) and transcriptional regulatory interactions (transcription factor binding sites; tfbs) (See Methods). To reconstruct the GRN, we chose transcriptomes from bladder tumor-derived epithelial cell lines in order to avoid any bias that would be introduced from using less homogenous transcriptomic data from bladder tumors that contains stromal genes. The resulting GRN was composed of 720 TFs/coTFs, 6 374 target genes and 31 003 regulatory interactions that were significantly enriched for validated ppis (*P*-value =6.34e-127) and tfbs (*P*-value<1e-100). Based on the shared targets of every pair of TFs/coTFs, the GRN was then transformed into a co-operativity network (co-regulatory BLCA-GRN).

Aiming to highlight the transcriptional program that would be active under an altered-*FGFR3* context, we calculated the activity of each TF/coTF using the CCLE expression data of only previously identified FGFR3-dependent bladder cancer cell lines bearing FGFR3 genomic alterations (translocations leading to fusion proteins or activating point mutations): RT112 (FGFR3-TACC3), RT112-84 (FGFR3-TACC3), RT4 (FGFR3-TACC3), SW-780 (FGFR3-BAIAP2L1) and UM-UC-14 (FGFR3-S249C). The computed activity was then projected on the inferred-BLCA-GRN (Figure 1A, left panel). To determine if the resulting network was also representative of human bladder tumors, we re-calculated the activity of the previously inferred TF/coTFs from two expression data sets of *FGFR3*-mutated tumors: 272 NMIBCs[9] and 52 MIBCs[10] (Figure 1A, right panel). We observed that many of the most active TF/coTFs (4th quartile, n = 74) in FGFR3-dependent bladder cancer cell lines were also active in both the FGFR3-mutated NMIBC and MIBC tumors (Figure 1B). However, we observed stronger similarities in the patterns of TF/coTF activity between the cell lines and the MIBC luminal papillary (LumP) and the NMIBC class 1. This could result from the fact that analyzed cell lines are derived from MIBC, and classified as luminal papillary, and NMIBC class 1 also present a luminal-like differentiation. Corroborating the relevance of our constructed network, we found several previously described bladder-cancer genes within the group of most active TFs/coTFs in these subgroups of luminal papillary tumors such as *GATA3*, *PPARG*, *FOXA1*, *KLF5*, *TRIM29* and *NOTCH3* (Figure 1B, left panel)[29–32]. The difference in the BLCA-GRN among tumors bearing an altered-*FGFR3* suggest that FGFR3 activity may depend on the molecular subtype, which could have clinical implications. However, 14 TFs/co-TFS are common in all subtypes and may be enriched in key elements of the altered-FGFR3 pathway (Figure 1B, right panel).

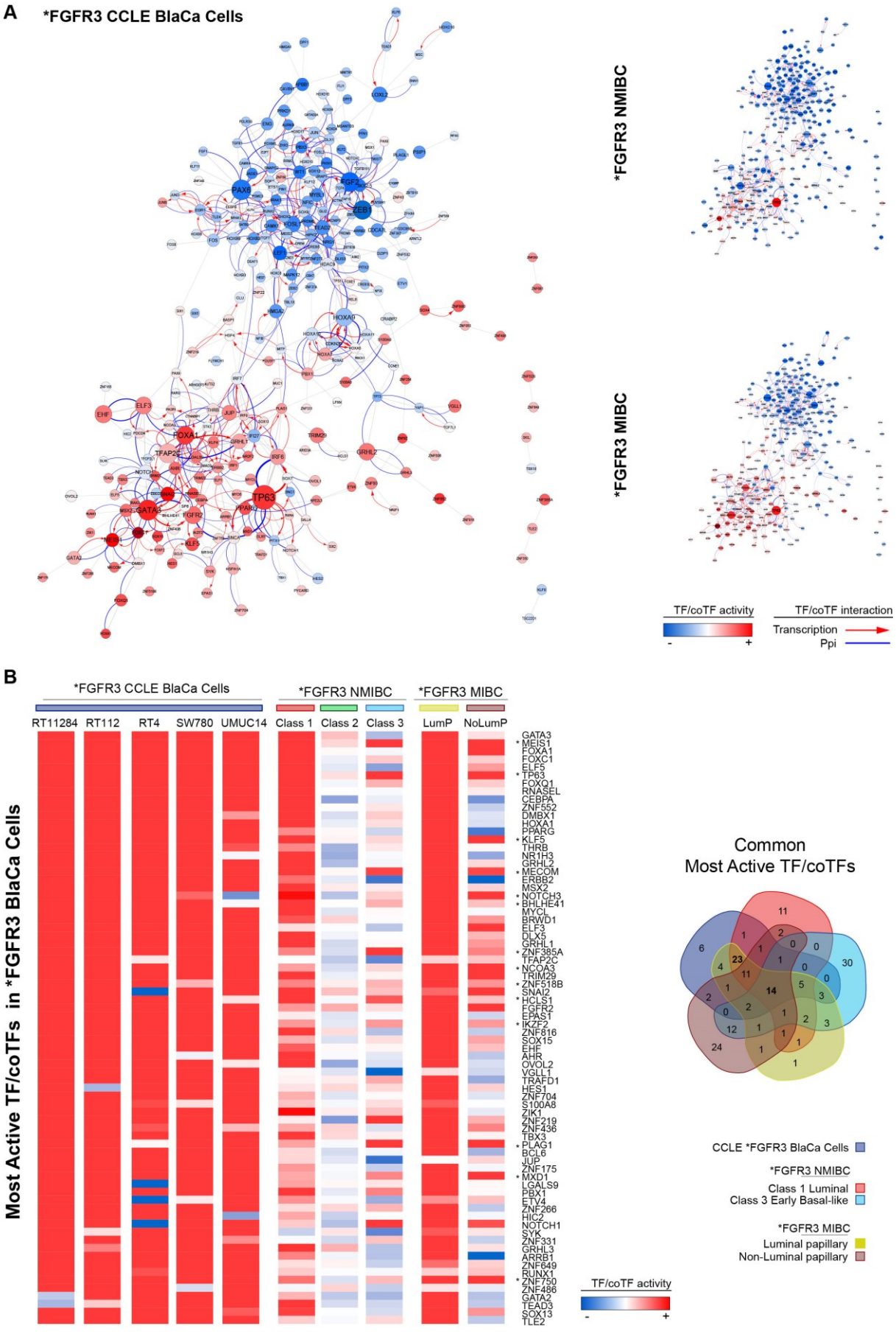
A
*FGFR3 CCLE BlaCa Cells
*FGFR3 NMIBC
*FGFR3 MIBC
TF/coTF activity
TF/coTF interaction
Transcription
Ppi
B
*FGFR3 CCLE BlaCa Cells
*FGFR3 NMIBC
*FGFR3 MIBC
RT11284
RT112
RT4
SW780
UMUC14
Class 1
Class 2
Class 3
LumP
NoLumP
Most Active TF/coTFs in *FGFR3 BlaCa Cells
GATA3
MEIS1
FOXA1
FOXC1
ELF5
TP63
FOXQ1
RNASEL
CEBPA
ZNF552
DMBX1
HOXA1
PPARG
KLF5
THRB
NR1H3
GRHL2
MECOM
ERBB2
MSX2
NOTCH3
BHLHE41
MYCL
BRWD1
ELF3
OLX5
GRHL1
ZNF385A
TFAP2C
NCOA3
TRIM29
ZNF518B
SNAI2
HCLS1
FGFR2
EPAS1
IKZF2
ZNF816
SOX15
EHF
AHR
OVOL2
VGLL1
TRAFD1
HES1
ZNF704
S100A8
ZIK1
ZNF219
ZNF436
TBX3
PLAG1
BCL6
JUP
ZNF175
MXD1
LGALS9
PBX1
ETV4
ZNF266
HIC2
NOTCH1
SYK
ZNF331
GRHL3
ARRB1
ZNF649
RUNX1
ZNF750
ZNF486
GATA2
TEAD3
SOX13
TLE2
TF/coTF activity
Common
Most Active TF/coTFs
CCLE *FGFR3 BlaCa Cells
*FGFR3 NMIBC
Class 1 Luminal
Class 3 Early Basal-like
*FGFR3 MIBC
Luminal papillary
Non-Luminal papillary

Figure 1.

Figure 1. Transcriptional co-regulatory network of FGFR3-altered bladder cancer cells and tumors.

A. ***Left Panel***. Co-operativity network inferred from the transcriptome of 36 bladder cancer derived cell lines (BLCA-GRN) and active only in altered-FGFR3 cells. Nodes represent transcription factors and co-factors (TFs/coTFs). The co-regulatory interactions between nodes are indicated as follows: solely defined by H-LICORN algorithm (gray) and interactions for which there is published evidence such as protein-protein interactions (ppi; blue) and transcriptional regulation (tfbs, red arrows). Node color (red= high; blue = low) represents the mean activity of the corresponding TF/coTF, estimated only from FGFR3-dependent bladder cancer cells (n=5). The size of nodes is proportional to the number of targets of a TF/coTF and the intensity of color to the activation value. ***Right*** **Panel.** Prediction of BLCA-GRN activity employing the transcriptome of human bladder tumors harboring a mutated-*FGFR3* (*FGFR3): Non-muscle invasive bladder carcinoma (NMIBC, n=272; EUROMOL; Upper Panel) and Muscle-invasive bladder carcinoma (MIBC, n=52; TCGA; Lower Panel). The meaning of size and color of nodes, as well as color of edges follows as described above.

B. **Left Panel.** Heatmap display of the most active (4th quartile) TFs/coTFs in FGFR3-dependent bladder cancer cell lines. Each column represents a transcriptomic dataset from which the sample-specific or mean activity of a corresponding TF/coTF (rows) was calculated. The significance of color used to represent TF/coTF activity is the same as described above: red; high activity, blue; low activity.
Right Panel. Venn Diagram analysis of each of the most active sets (4th quartile) of TFs/coTFs in five transcriptomic datasets of FGFR3-altered samples: CCLE cell lines, NMIBC of Class 1 and of Class 3, and MIBC of luminal-papillary and non-luminal-papillary subtype. The 14 common most active TFs/coTFs are highlighted on the heatmap by an asterisk.

Essential FGFR3-driven TFs and coTFs in bladder cancer.

To experimentally evaluate part of the inferred co-regulatory BLCA-GRN in tumors bearing an *FGFR3*-alteration, we performed a TF Activation Profiling Plate Array assay on UM-UC-14 cells treated or not with the pan-FGFR inhibitor PD173074 (Figure 2A, right panel). The Array allowed to analyze the activity of 10 out of 74 of the regulators (or family members of the regulators) defined by CoRegNet as being the most active in UM-UC-14 cells (Figure 2A, left panel). Validating part of the predicted co-regulatory network, the inhibition of FGFR3 in UM-UC-14 cells led to a significant decrease in the target DNA sequence binding of all of the 6 TFs/family members of TFs representing in total 9 of the most active regulators in UM-UC-14 cells (Figure 2A, right panel).

Having confirmed at a small scale the reliability of prediction of CoRegNet, we continued to use this tool to compute the activity of the inferred BLCA-GRN regulators using other experimentally derived transcriptomic datasets to identify regulators activated in an altered-FGFR3 context and driven by this receptor. We compared the GRN after inhibition or activation of FGFR3 (Figure 2B). We used publicly available transcriptomic data from MGH-U3 and RT112 cells treated or not with the pan-FGFR3 inhibitor AZD4547 for 2, 6 and 24 hours, and our transcriptomic data from bladder tumors and hyperplasia from mice overexpressing in urothelial cells a human *FGFR3* presenting the S249C mutation, and from littermate control urothelium. We proceeded by first calculating the activity of every TF/coTF in each independent dataset and then focusing on those regulators that presented an opposite activation status between the FGFR3 inhibited bladder cancer cell lines and the

murine bladder tumors overexpressing a constitutively active hFGFR3-S249C (Figure 2B; *n* = 25 TF/coTFs). To determine if such FGFR3-driven regulators were essential elements of the network for FGFR3's oncogenic activity, we evaluated the impact that the knockout of one of such genes would have on the cell viability of FGFR3-dependent bladder cancer cell lines using publicly available data from the high-throughput screening of gene dependencies (Broad Institute, AVANA CRISPR-Cas9 dataset) (Figure 2C). Amongst the few TFs that were identified as being essential for FGFR3-dependent cell lines were TP63 and FOXM1. Strikingly, the knockout of *TP63* (encoding p63) had the strongest impact on cell viability of FGFR3-dependent bladder cancer cells and this impact was greater compared to wt (wild-type) *FGFR3* cells despite a well-established role of p63 in squamous/ basal tumors in general and basal MIBC in particular [33–35](Figure 2C).

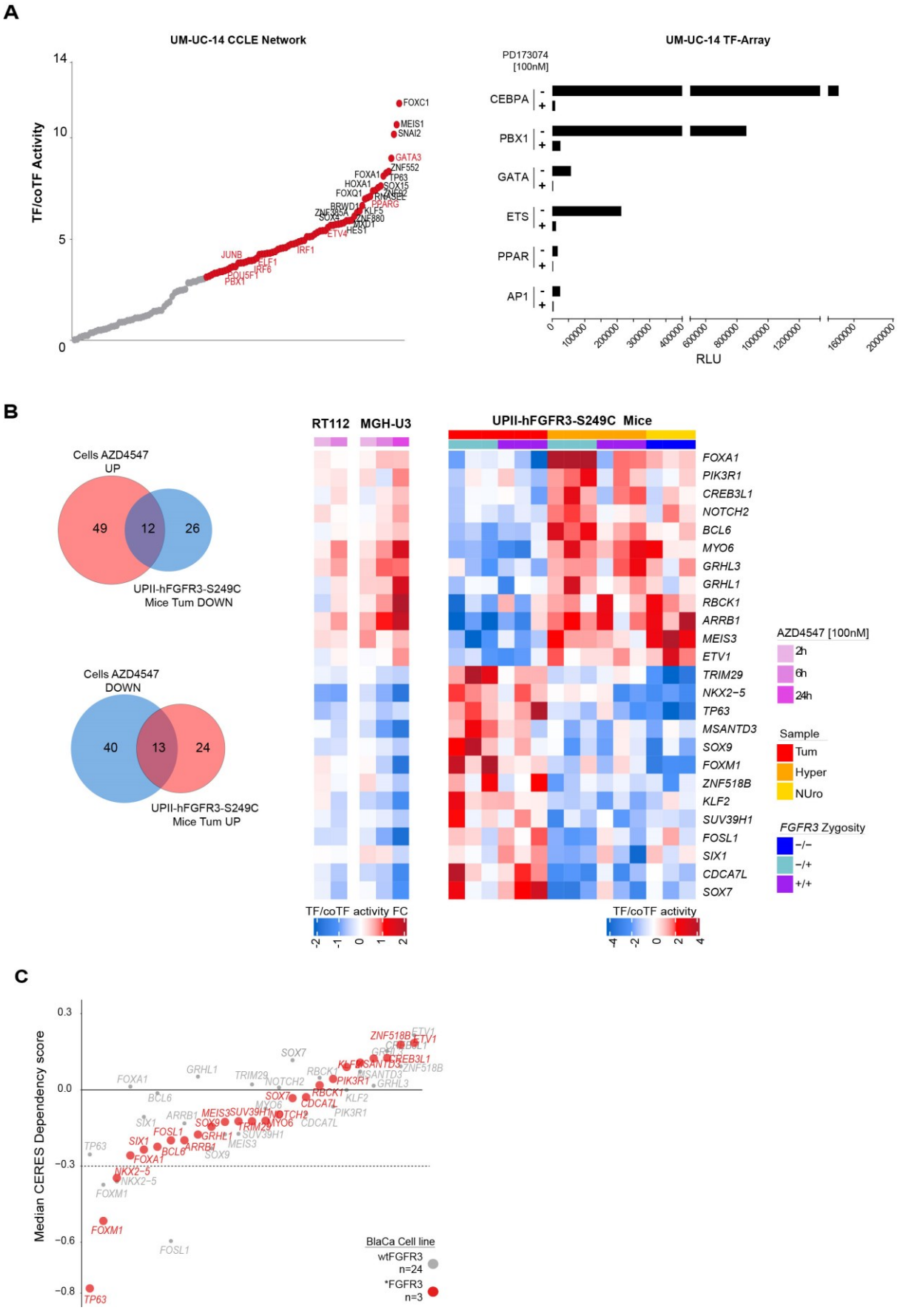
A
UM-UC-14 CCLE Network
TF/coTF Activity
FOXC1
MEIS1
SNAI2
GATA3
ZNF552
FOXA1
TP63
HOXA1
SOX15
FOXQ1
PPARG
BRWD1
KLF5
ZNF880
HOXD1
HES1
ETV4
IRF1
JUNB
ELF1
IRF6
POU5F1
PBX1
UM-UC-14 TF-Array
PD173074
[100nM]
CEBPA
PBX1
GATA
ETS
PPAR
AP1
RLU
B
RT112
MGH-U3
UPII-hFGFR3-S249C Mice
Cells AZD4547
UP
49
12
26
UPII-hFGFR3-S249C
Mice Tum DOWN
Cells AZD4547
DOWN
40
13
24
UPII-hFGFR3-S249C
Mice Tum UP
FOXA1
PIK3R1
CREB3L1
NOTCH2
BCL6
MYO6
GRHL3
GRHL1
RBCK1
ARRB1
MEIS3
ETV1
TRIM29
NKX2−5
TP63
MSANTD3
SOX9
FOXM1
ZNF518B
KLF2
SUV39H1
FOSL1
SIX1
CDCA7L
SOX7
AZD4547 [100nM]
2h
6h
24h
Sample
Tum
Hyper
NUro
FGFR3 Zygosity
−/−
−/+
+/+
TF/coTF activity FC
TF/coTF activity
C
Median CERES Dependency score
BlaCa Cell line
wtFGFR3
n=24
*FGFR3
n=3

Figure 2.

Figure 2. Identification of FGFR3-regulated TFs and coTFs in bladder cancer: discovery of TP63 as an essential gene.

A. Left Panel. TFs/coTFs exhibiting a positive activity calculated from the BLCA-GRN and the transcriptome of the UM-UC-14 cell line. Colored in red are the most active (4th quartile; n=74) regulators. Names of the top 20 most influent regulators are shown. Regulators whose names are further highlighted in red are those that were partially validated using a TF array in 2B.
Right Panel. Activation levels of the TFs or TF families present in a TF activation profiling plate array, and representing 10 out of the 74 most active TFs/coTFs in UM-UC-14 cells. UM-UC-14 cells were treated or not with a pan-FGFR inhibitor (PD173074) and TF activity levels were measured as the enrichment of bound TF/probes. Activity profiles that present more than two-fold change between experimental samples are considered significant. RLU: Relative Luminescence Units.

B. Left Panel. Venn diagram of the TFs/coTFs of the BLCA-GRN whose estimated activity presents a change following the perturbation of FGFR3 in two transcriptomic datasets: (i) RT112 and MGHU3 treated with FGFR3 inhibitor (AZD4547) and (ii) bladder tumors derived from mice overexpressing a human FGFR3 (S249C) specifically in the urothelium. Focus is made on those regulators presenting an opposite and coherent change of activity following the inhibition or overexpression of FGFR3 in the two preclinical models (n=25).
Right Panel. Heatmap display of the 25 commonly deregulated TFs/coTFs and their sample-specific activity (murine tumors; red: high; blue: low), or fold change (FC) of activity with respect to control (cell lines; comparison to untreated cells).

C. Impact on cell viability (CERES dependency score) of altered-FGFR3 (red) and non-altered-FGFR3dependent bladder cancer cell lines upon KO (CRISPR-Cas9 AVANA database, Broad Institute) of one of the 25 common TFs from 2C.

P63 is regulated by FGFR3 and regulates cell proliferation

After examining our BLCA-GRN, we decided to focus the rest of the study on the transcription factor p63 as 1) it was one of the 14 genes found to be activated in both cell lines and FGFR3-altered tumors, independently of the subgroups; 2) it was found to be controlled by altered-FGFR3 and 3) it was essential for FGFR3-dependent bladder cancer cell viability in the AVANA screen.

Firstly, we investigated whether the regulation of p63 activity was due to a modulation of its protein levels by an altered-FGFR3 via the treatment of MGH-U3 (FGFR3-Y375C), UM-UC-14 (FGFR3-S249C) and RT112 (FGFR3-TACC3) bladder cancer cells with the pan-FGFR inhibitor PD173074. Western blot analysis showed a decrease of p63 levels in all three cell lines following the inhibition of FGFR3 (Figure 3A, left panel) without affecting the cellular localization of p63 (Supplementary Figure 1A). Supporting the relevance of these results in human tumors, the levels of p63 were also diminished after the anti-FGFR treatment of a patient derived xenograft (PDX) model harboring an FGFR3-S249C (Figure 3A, right panel). A kinetics of FGFR3 inhibition in RT112 cell lines revealed that the effect of FGFR3 inhibition on p63 levels was observed only at longer treatment times, suggesting that the regulation of p63 may occur at the transcriptomic level, rather than via the stabilization of the protein via the prevention of its degradation by proteasome (Supplementary Figure 1B). Analysis of transcriptomic data obtained after FGFR3 knockdown in MGH-U3 cells identified indeed a significant decrease of TP63 mRNA levels[20]. Further supporting this transcriptomic regulation of *TP63* by FGFR3, analysis of mRNA levels in human bladder tumors showed

that *TP63* expression was significantly higher in both NMIBCs and MIBCs mutated for *FGFR3* (Figure 3B). Additionally, a significant positive correlation was found between *FGFR3* and *TP63* mRNA levels in both tumor subgroups, independent of *FGFR3* status (NMIBC cor 0.57, pval=6.59e-10; MIBC cor 0.50, pval=1.34e-07; Pearson's correlation). Knowing that there exist many different isoforms of *TP63*, which can have different activities, we verified by RT-qPCR that the ΔNP63 isoform was the dominant isoform expressed in both our human bladder tumors and bladder cancer derived cell lines, whatever the FGFR3 mutation status (Supplementary Figure 1C-D).

To corroborate the dependency of FGFR3-mutated bladder cancer cells on p63 observed in the AVANA CRISPR-Cas9 publicly available data (Figure 2C), we invalidated *TP63* expression using siRNA in MGHU-3 and UM-UC-14 cells. Knockdown of *TP63* by three independent siRNAs led to a significant decrease of cell viability in both FGFR3-dependent cell lines (Figure 3C and Supplementary Figure 2A). To evaluate the role of p63 in 3D culture, *in vitro* and *in vivo*, we developed stables clones of inducible-shTP63 (shTP63i) transduced MGH-U3 and UM-UC-14 cells. Doxycycline (Dox) treatment of both shTP63i cells induced a knock-down by ca. 50% of protein expression (Supplementary Figure 2B-D) and significantly impaired cell growth in a 3D culture spheroid model (Figure 3D, Supplementary Figure 2C). Moreover, doxycycline treatment of a xenograft model derived from the shTP63i MGHU-3 cell line led to a significantly stunted tumor growth compared to the untreated control mice (Figure 3E). A reduction in the number of proliferating cell nuclear antigen (PCNA) positive cells was observed in absence of p63, indicating that p63 regulated cell proliferation of FGFR3-dependent cells (Figure 3F, Supplementary Figure 2E).

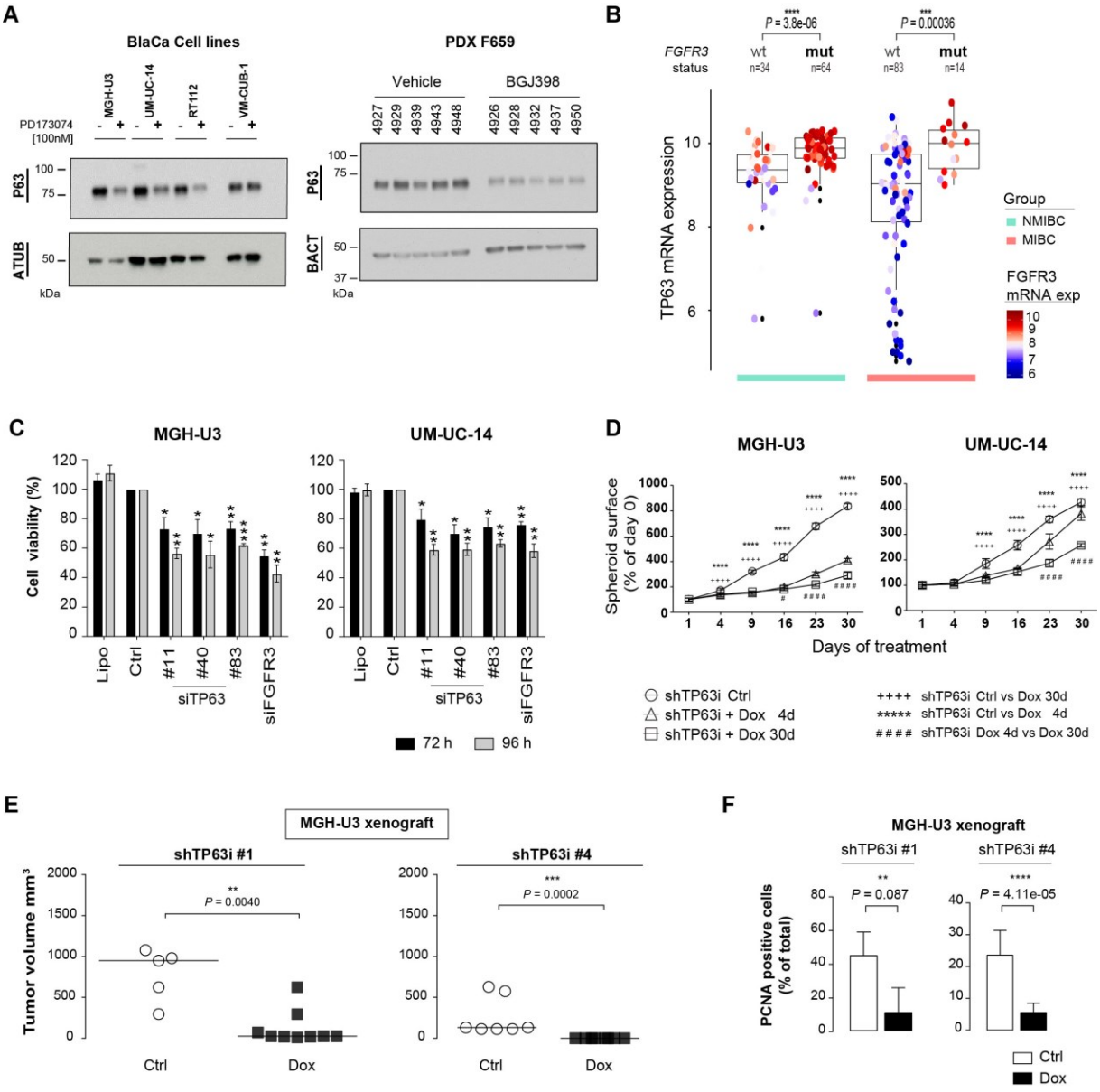

Figure 3. Regulation of *TP63* expression and impact of its knockdown on cell proliferation in an altered-FGFR3 context.

A. Western blot of p63 after anti- FGFR3 treatment of MGHU-3 and UM-UC14 cells (PD173074 100nM, 40h) or tumors derived from a mutated-FGFR3 PDX model (BGJ398 30mg/kg/day ,4 days). Actin (BACT) was used as loading control. The blot for MGH-U3 and UM-UC-14 is representative of three independent experiments. VM-CUB1 cells expressing a wt*FGFR3* were used as control.

B. Comparison of *TP63* mRNA expression levels in the CIT cohort of NMIBC (*n* = 98) and MIBC (*n* = 97) human bladder tumors, subdivided according to *FGFR3* mutational status (wt: wildtype; mut: mutated). Each dot represents an individual sample and the color of the dot is proportional to the centered mRNA expression of *FGFR3* per sample.

C. Cell viability assay (Cell Titer-Glo) evaluating the effect of TP63 knockdown (siRNA) in MGH-U3 and UM-UC-14 cells 72 and 96 hours after transfection.

D. Cellular spheroids were established from MGH-U3 and UM-UC-14 cells stably transduced with a Dox-inducible shTP63 (shTP63i). 3D cell growth was analyzed at different stages following the knockdown of *TP63*, induced after doxycycline (Dox) treatment. Spheroids received Dox-treatment either for a long period (30 days) to keep a stable knockdown of *TP63* or for a short period (4 days) to induce a transient knockdown of *TP63* and allow for recovery of expression after. Statistical comparison was done by a 2-way ANOVA.

E. Murine xenograft tumors were derived from two clones of MGHU-3 bladder cancer cells stably expressing a Dox-inducible shRNA targeting *TP63* (shTP63i#1, shTP63i#4). Xenografted mice received or not doxycycline in the drinking water (Dox;1g/L) for 30 days. Tumor growth was assessed every twice a week. Data is expressed as final tumor volume at the end of treatment. Each dot represents an individual sample. Statistical comparison was done by Wilcoxon's test.

F. Quantification of proliferating nuclear cell antigen (PCNA) immunostaining in tumors of xenografted mice from 3E (MGH-U3 shTP63i#1: Ctrl *n* = 6, Dox *n* = 6; MGH-U3 shTP63i#4: Ctrl *n* = 9, Dox *n* = 9). Statistical comparison was done by Wilcoxon's test.

p63 favors migration and invasion of FGFR3-dependent bladder cancer cells.

To further assess the functional relevance of p63 within an altered-FGFR3 context in bladder cancer, we generated a p63 target gene signature from MGH-U3 cells. Possible direct transcriptional targets of p63 were investigated by chromatin immunoprecipitation of p63, combined with massive parallel sequencing (ChIP-seq). P63-ChIP-seq of two independent MGH-U3 replicates unveiled 6 000 potential p63-binding sites at a distance +/- 5kb from the transcriptional start site (TSS) of the target gene (Supplementary Figure 3A). We then integrated these results with the RNA-seq expression profiling of siTP63 transfected MGH-U3 cells to define which of the putative target genes were effectively regulated following the knockdown of *TP63* (Supplementary Figure 3B). Gene ontology (GO) enrichment analysis of the p63 direct target genes revealed that p63 positively mediates cellular processes such as cell migration, invasion and proliferation, and represses cellular death (Supplementary Figure 3C).

This transcriptomic analysis corroborated with what we already observed for the role of p63 in regulation on cell proliferation. We then aimed at validated experimentally the role of p63 in mediating cell migration and invasion. Treatment of sh*TP63*i UM-UC-14 cells with doxycycline significantly blunted cell migration as analyzed by a wound healing assay (Figure 4A). Membrane-type I-matrix metalloproteinase (MT1-MMP) plays a central role in pericellular matrix degradation during local invasive programs and metastasis[36]. An association between p63 and MT1-MMP has already been reported in other models[37]. Here we observe that silencing of *TP63* led to a significant reduction of gelatin degradation in both shTP63i transduced MGH-U3 and UM-UC-14 cells indicating that MT1-MMP activity is p63 dependent (Figure 4B-C). Underlying this process, the expression of membrane-type I-matrix metalloproteinase (MT1-MMP) was decreased upon *TP63* depletion in MGH-U3 shTP63i cells (Figure 4D). Nonetheless, the exact role of MT1-MMP in such processes in bladder cancer would need to be further studied. Overall, these results demonstrate that p63 mediates both cell migration and invasion through the degradation of extra-cellular matrix in FGFR3-dependent cells.

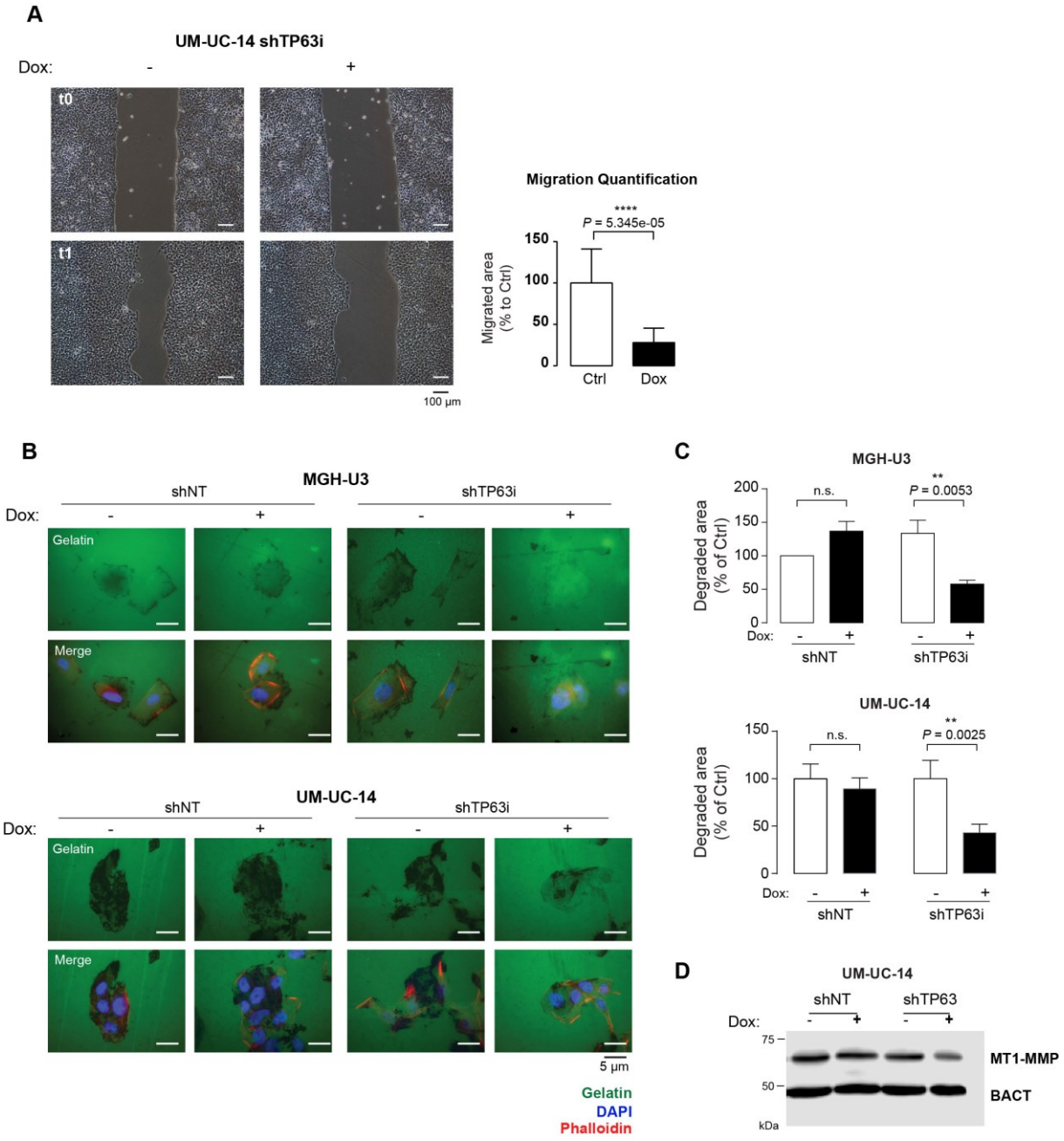

Figure 4. Functional consequences of TP63 gene invalidation in FGFR3-dependent bladder cancer cells: Effect on cell migration and invasion.

A. Wound healing assay to measure cell migration of UM-UC-14 shTP63i#4 cells after the doxycycline (Dox)-induced knockdown of *TP63*. Left Panel: representative images depicting the scratch (wound) at time 0 (t0) and 24 hours (t1) post-scratching. Scale bar is equivalent to 100µm. Right panel: Relative wound area was measured at both times to define the percentage of migrated area with respect to Dox-untreated, control cells. Data is expressed as mean ± SD. Statistical differences were defined by a Wilcoxon's test.

B. Degradation of Alexa 488 gelatin by MGH-U3 shTP63i#4 and UM-UC-14 shTP63i#4 cells treated or not with Dox to induce *TP63* knockdown. Scale bar is equivalent to 5µm.

C. Quantification of degraded gelatin from 3B. Results are expressed as mean ±SD of triplicate samples. The two-way ANOVA test was employed to statistically compare groups. shNT: non-targeting shRNA.

D. Western blot of MT1-MMP and β-ACTIN (BACT; loading control) in UM-UC-14 cells transfected with a control (shNT) or *TP63* targeting shRNA, inducible by doxycycline (Dox) treatment.

P63 activation levels are higher in NMIBC bearing FGFR3 alterations and could be associated to the higher tendency of recurrence in these tumors.

Given the key roles of p63 in FGFR3-dependent *in vitro* models, we then further investigated if p63 activity was specifically induced by mutated-FGFR3 and associated with tumor prognosis assuming that its role in migration could favor tumor recurrence. Based on the study by Hernandez *et al* [38], we focused on Ta NMIBC tumors that were reported to be enriched in FGFR3 mutations and which presented higher recurrence for certain tumor subgroups. Employing our BLCA-GRN and the UROMOL transcriptomic dataset of NMIBC[9], we inferred the activity of p63 in the 289 Ta NMIBCs and identified both a significantly higher activity of p63 and a higher tendency of recurrence in mutated-FGFR3 tumors compared to wild-type (Figure 5A-B). These results suggest that p63 may participate in tumor recurrence in a mutated-FGFR3 context.

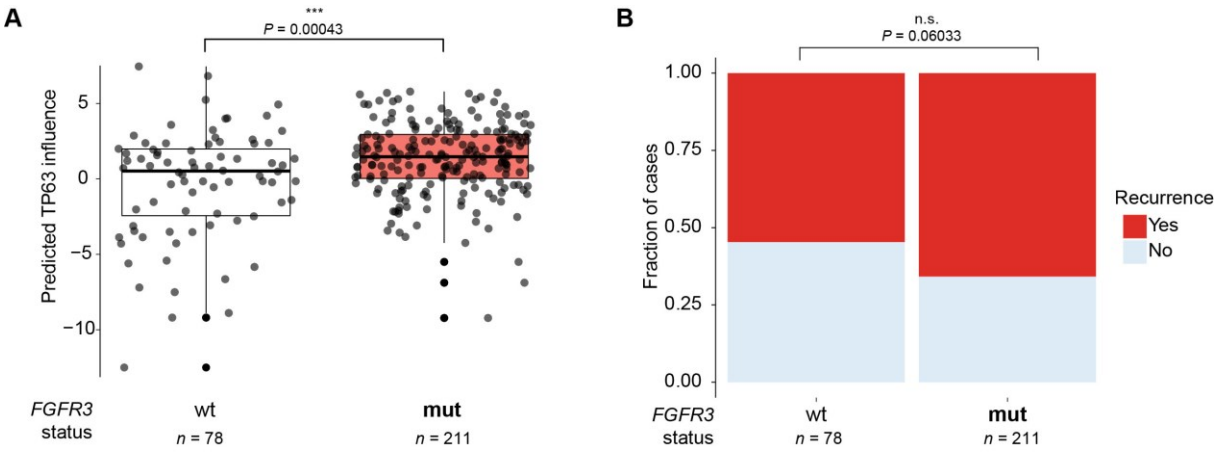

Figure 5. P63 activity levels in FGFR3-mutated NMIBC human tumors.

Activity levels of p63 were predicted from the BLCA-GRN and the UROMOL transcriptomic dataset of human Ta NMIBC tumors. Comparison of activation status was done by grouping samples in different ways:

A. Activity levels of p63 in Ta NMIBC (UROMOL) as calculated using the predicted BLCA-GRN. Tumors were separated according to *FGFR3* mutational status (wt: wildtype; *n* = 78, mut: mutated; *n* = 211). Tumors not presenting any information regarding *FGFR3* status were excluded. Each dot represents an individual sample. Wilcoxon's test was used for statistical comparison between groups. Data are expressed as mean ± SD

B. Proportion of recurrence events in wildtype versus mutated-FGFR3 Ta NMIBCs. Fisher's exact test was carried out to evaluate statistical differences between groups.
Number of tumors belonging to each group is indicated under each graph.

Discussion

In summary, through a reverse-engineering method, we have presented here the first bladder-cancer specific gene regulatory network, inferred without any *a priori* knowledge. By using the H-LICORN algorithm and the CoRegNet package, we were able to extract a network of co-operative regulators (TFs/coTFs) whose interactions were refined using regulatory evidences from different data sources. A major reason to focus our study on co-operative TFs/coTFs is that disease phenotypes; including those related to disease progression and response to therapy, have been demonstrated to be maintained by small groups of TFs and coTFs [39,40]

To produce a more reliable GRN, we inferred our network using a more homogenous transcriptomic dataset from bladder cancer cell lines and subsequently demonstrated that it was also relevant to both NMIBC and MIBC bladder tumors. Notably, many of the regulators forming part of the network were previously associated to bladder cancer and/or urothelial differentiation such as *FOXA1*, *PPARG*, *GATA3*, *TP63* [10,41,42] emphasizing the biological representativity of the inferred BLCA-GRN. However, when using transcriptomic data from our FGFR3-induced mouse model of BLCA and for FGFR3-bladder cancer cell lines after FGFR3 inhibition, we were able to identify some key TFs such as FOXM1 (Figures 2B and 2C) that were not identified from the human FGFR3. We were also not able to validate some previously described key regulators of bladder cancer such as MYC involved in a FGFR3

regulatory-loop[20]. This is partly because the algorithm used will infer a GRN only from TFs/coTFs that have a significant variation of expression across the samples in the input data. MYC and FOXM1 do not necessarily vary at the level of mRNA, but are rather controlled at a pos-translational level. Such unavoidable limitation, inherent to other GRN reconstruction algorithms[25], stresses the importance to use both bioinformatic and experimental approaches to construct GRNs. In this study, by employing transcriptomic data originating from different sources (patient samples and experimental data), we have constructed and validated a GRN characteristic of an altered-FGFR3 context in bladder tumors.

Our analysis showed that the TFs/coTFs activated by FGFR3 were different depending of the molecular tumor subtypes suggesting a context-specific activity of a mutated-FGFR3 which could be involved in the low response rate of FGFR3-altered tumors to anti-FGFR3 therapies (37% partial response and only 3% complete response)[6].

Among the BLCA-GRN TFs/coTFs being driven by an altered-FGFR3 in all experimental datasets, we surprisingly uncovered the p63 transcription factor. Whereas the role of p63 has been already clearly demonstrated in a bladder cancer in a basal molecular context[29,33–35], there exist few reports investigating the role of this transcription factor in the more differentiated, luminal subtype of bladder tumors (enriched for FGFR3 alterations). Of note, whilst this hyperactivation of a p63 regulon was already described in luminal papillary MIBC, no direct link with FGFR3 was made[41]. In this study we demonstrated that the expression of p63 is regulated by FGFR3 in bladder cancer cell lines and PDX models. Analysis of its functional role confirmed that p63 is an essential TF mediating cell proliferation, migration and invasion of FGFR3-dependent bladder cancer cell lines.

Considering that p63 is able to drive an invasive program in the more aggressive basal bladder cancer subtypes[29,35,43,44], it is striking to observe that it similarly regulates migration/invasion in an altered-FGFR3 context, a context associated to NMIBCs or luminal-like MIBCs. In human bladder tumors, we observed a significantly stronger p63 activation in mutated-FGFR3 NMIBC tumors, associated to a tendency of higher recurrence rate of this mutated-tumors. This led us to hypothesize that p63-induced migration of FGFR3-mutated cells could favor recurrence. The fact that we observed a higher tendency but not a statistical difference of recurrence between mutated-FGFR3 tumors and wild-type tumors suggests that p63 may not be the only player favoring this process. It will be important to further study the functional network of p63 in different subtypes of FGFR3-mutated tumors.

Previous studies have reported that a loss of p63 is associated to a worse outcome (higher recurrence and/or progression) in NMIBC patients[35,45–49]. This would appear at first as contradictory to our findings revealing a possible association between a higher p63 activity and higher tumor recurrence in certain NMIBC subtypes. A possible explanation of such

discrepancies of results could be linked to the fact that in the former studies, protein expression levels were measured whereas we measured p63 activity through a transcriptomic analysis. Moreover, knowing that p63 may exert opposite functions depending on the cellular background[50,51], it is important to more deeply study its context-specific regulation in order to propose therapeutic strategies suited to distinct clinical scenarios.

In this study we have focused on the functional validation of p63, one of the putative essential regulators driven by FGFR3 in bladder tumors. However, our work provides a bladder-cancer-specific GRN that enables the identification of TFs and coTFs that are essential in an altered-FGFR3 context, and that could be studied more in depth to improve current therapeutic options and increase our understanding of bladder cancer biology.

Materials and Methods

Public Data Collection

Human bladder cancer cell transcriptome (RNA-seq) and *FGFR3* mutational status corresponding to 36 bladder cancer cell lines (5 cell lines were mutated for *FGFR3* and were dependent on its signaling) were collected from the Cancer Cell Line Encyclopedia (CCLE DepMap 2019Q1, Broad Cancer Dependency Map Project)[52].

Bladder tumor transcriptome (RNA-seq) was collected from two large cohorts of NMIBC and MIBC. NMIBC transcriptome and *FGFR3* mutational status were collected from the published dataset by Hedegaard *et al* (ArrayExpress E-MTAB-432)[9] corresponding to 476 tumors (272 tumors presented a mutated *FGFR3*). The same data (RNA-seq) corresponding to the MIBC cohort was collected from the The Cancer Genome Atlas (TCGA) dataset (cbioPortal)[10] of 408 tumors (52 tumors presented a mutated *FGFR3*).

Gene invalidation (CRISPR-Cas9; CERES dependency score) large screen data to identify essential genes in human cancer cell lines (27 bladder cancer cell lines) was collected from the AVANA genetic dependency dataset (AVANA 2019Q3, Achilles Project, Broad Institute)[28].

Transcriptomic data (Human Affymetrix DNA Array U133 Plus 2) of MGH-U3 and RT112 cells treated with AZD459 [100nM] were recovered from the Array Express E-MTAB-4749 dataset[53].

Inference of the gene regulatory network (GRN)

As a first step, a bladder-cancer-specific GRN was constructed from the CCLE human bladder cancer cell line transcriptome (n=36 bladder cancer cells) using the Bioconductor CoRegNet package[27]. The CoRegNet package implements the hybrid learning co-operative regulation networks (H-LICORN) algorithm[26] to infer a series of gene regulatory networks (GRN) from transcriptomic data and a list of previously defined regulators. The list of known regulators (transcription factors and co-factors; TFs/coTFs; n=2375) is defined from previously published datasets by Lambert *et al* and Schmeier *et al* [54,55]. In summary, H-LICORN infers the best GRN that describes the regulatory interactions between regulators and their target genes through four steps: (1) First, the transcriptomic matrix is discretized into -1, 0 and 1 values that fit its per-gene distribution of expression. In addition, genes present in the transcriptome matrix are classified into regulators and target genes and only those presenting a significant variation in expression levels across samples are kept. (2) Second, potential sets of co-activators and co-repressors regulating the expression of a target gene are determined through frequent items search techniques. (3) Third, for each target gene, a list of the candidate co-activators and co-inhibitor sets (GRN) is selected by employing an association rule metric (based on gene regulation). (4) Next, such sets of GRNs are scored following a regression model between the expression of the regulators forming part of the GRN set and the expression of their target genes. For each target gene, the top 10 GRN candidate sets presenting the best R^2 score are kept. CoRegNet can additionally refine the inferred GRN by integrating published interaction evidences such as protein-protein interactions [HIPPIE[56], STRING[57], FANTOM, iRefR HPRD[58]] and transcription factor binding sites (ChEA2[59]; ENCODE ChIP v3, Motif Db Bioconductor; HOCOMOCO[60], ITFP, ENCODE, Neph2012, TRRUST, Marbach 2016[61], TRED[62]]. Each GRN is given a score that merges the previous R^2 score and a score representing validated regulatory interactions. The GRN with the maximum final merged score is selected and it is then transformed into a co-regulatory network based on the shared target genes between the inferred regulators.

Estimation of sample-specific TF/coTF activity

Using the CoRegNet package, we further computed a network-based regulatory influence that represents an estimated activity for each TF/coTF having a sufficient number of gene targets, for each transcriptome sample. Briefly, the measure of influence estimates the activity of a TF/coTF based on a Welch t-test comparing the distribution of expression of the set of activated and repressed target genes for each TF/coTF in each individual sample. In addition, an advantage of the CoRegNet package is that one may compute the TF/coTF influence for many different datasets using the regulatory information of one same GRN. In

this study, we constructed a bladder-cancer specific GRN, and then calculated the influence of the inferred TF/coTFs using transcriptomic data from different sources.

Validation of the FGFR3-GRN

Using the inferred bladder-cancer specific GRN, we calculated the influence of the predicted TFs/coTFs using transcriptomic data of preclinical models where the activity or gene expression of FGFR3 was altered. The first dataset used was the E-MTAB-4749 transcriptomic data from MGH-U3 (FGFR3-Y375C) and RT112 (FGFR3-TACC3) bladder cancer cell lines treated with the FGFR pan-inhibitor AZD4547 [100nM, 2,6,24h][53]. The second dataset was the human orthologue transcriptomic data of FGFR3-induced murine bladder tumors (murine model of hFGFR3-S249C overexpression in the urothelium) [Moreno-Vega, Shi, Fontugne, Meng 2019 unpublished]. The most influent TFs/coTFs additionally presenting an opposite and coherent activity between the FGFR3-inhibited and FGFR3-overexpressed preclinical models were taken as FGFR3-driven regulators.

Visualization of the GRNs

Visualization of the constructed networks and overlay of the computed influence and regulatory interactions was done using Cytoscape[63].

Cell culture

Human bladder cancer derived cell lines were obtained from different repositories: RT112, UM-UC-14 and VM-CUB-1 were obtained from DSMZ (Heidelberg, Germany); SW-780 cells were obtained from ATCC (Virginia, United States); UM-UC-5 were obtained from the ECACC collection (Porton Dow, England) and MGH-U3 and RT4 were kindly supplied by Dr. Francisco X. Real. The MGH-U3 and UM-UC-14 harbor the Y375C and S249C FGFR3 mutation respectively. RT112 and RT4 express the FGFR3-TACC3 translocation, whereas the SW780 present the FGFR3-BAIAP2L1 translocation. UM-UC-5 and VM-CUB-1 express a wildtype *FGFR3*. MGH-U3, UM-UC-14, UM-UC-5 and SW-780 were cultured in DMEM whilst RT112 and RT4 were cultured in RPMI. All culture media were supplemented with 10% fetal bovine serum. Cell culture was carried out at 37°C under a 5% CO_2 atmosphere.

FGFR3 inhibition in vitro

MGH-U3, RT112, RT4, SW-780, UM-UC-14, UM-UC-5 and VM-CUB-1 cell lines were seeded in 100mm plates at the following respective total densities: $5.0x10^6$, $4.0x10^6$, $4.5x10^6$, $1.8x10^6$, $3.0x10^6$, $5.0x10^6$, $1.8x10^6$ and $0.8x10^6$ cells/100mm dish. Cells were plated and left to adhere overnight. Thereafter, cells were treated for 40 hours with the pan-FGFR inhibitor PD173074 [100nM] (Calbiochem, Merck Eurolab, France). Control cells were treated with

DMSO vehicle diluted in the same way as the inhibitor. At the end of treatment, whole cell lysates or nuclear and cytosolic cell fractions were recovered for immunoblotting. Cellular fractions were obtained using the Thermo Fisher NE-PER nuclear and cytoplasmic extraction kit (ref 78833), according to the manufacturer's protocol.

Transcription Factor Activity Array

The activity of 48 families of transcription factors was analyzed from the isolated nuclear extracts obtained from UM-UC-14 cells treated or not for 40 hours with 100nM PD173074 using the TF Activation Profiling Plate Array I kit from Signosis (following the manufacturer's instructions).

Gene knockdown and cell viability assays

MGH-U3 and UM-UC-14 cells were transfected for 48, 72 and 96 hours with 5nM siRNA together with Lipofectamine RNAi Max reagent (Invitrogen) as indicated in the manufacturer's protocol. For protein or RNA analyzes, cells were plated in six-well plates at a seeding density of 300 000 cells/well for MGH-U3 cells and 150 000 cells/well for UM-UC-14 cells and cells were lysed at 48h after transfection with appropriate lysis buffer. For cell viability assays, cells were plated in ninety-six well plates at a seeding density of 10 000 cells/well for MGH-U3 cells and 5 000 cells/well for UM-UC-14 cells and cell viability was measured (Cell Titer Glo, Promega) at 72 and 96 hours.

Three different TP63 siRNA (TP63 siRNA #11, #40, #83; Ambion Silencer select, ThermoFisher Scientific) were used and a siRNA targeting FGFR3 was used as a positive control (Qiagen). As negative controls, we used an siRNA directed against luciferase (Qiagen SI03650353) and the non-targeting negative control Silencer Select (Thermo Fisher Scientific
4390846). The sequences of siRNAs employed are as follows:

	Strand	Sequence 5'-3'
TP63 #11 ref (4392420 s16411)	sense	GGAUGAAGAUAGCAUCAGA
	anti-sense	UCUGAUGCUAUCUUCAUCC
TP63 #40 ref (4392420 s229400)	sense	GAACCGCCGUCCAAUUUU
	anti-sense	UAAAAUUGGACGGCGGUU

TP63 #83 ref (4392420 s531583)	sense	UGAUGAACUGUUAUACUU
	anti-sense	UAAGUAUAACAGUUCAUCA
FGFR3 #4 ref (4392420 s5168)	sense	CCUGCGUCGUGGAGAACAATT
	anti-sense	UUGUUCUCCACGACGCAGGTG

Real-time reverse transcription quantitative PCR

RNA from bladder cancer cell lines was extracted with Qiagen's RNA easy minikit, in accordance to the manufacturer's protocol. RNA from our human bladder tumor cohort was extracted through cesium chloride density centrifugation as mentioned further on.

Reverse transcription was performed with 1µg of total RNA employing the High-Capacity cDNA reverse transcription kit (Applied Biosystems). cDNAs were subsequently amplified by PCR in a Roche real-time thermal cycler with the Roche *Taq*man master mix and the following master probe primers:

Gene	Strand	Sequence 5' - 3'	Roche T*aq*man probe
ΔNp63	sense	GGTTGGCAAAATCCTGGAG	No. 56
	antisense	GGTTCGTGTACTGTGGCTCA	
18s rRNA	sense	GGAGAGGGAGCCTGAGAAAC	No. 8
	antisense	TCGGGAGTGGGTAATTTGC	

Immunoblotting

Protein extraction of MGH-U3, RT112, RT4, SW-780, UM-UC-14, UM-UC-5 and VM-CUB-1 cell lines was done through cell lysis in Laemmli buffer (50 mM pH 6.8 Tris-HCl, 2.5 mM EDTA, 2.5 mM EGTA, 2 mM DTT, 5% glycerol, 2% SDS) supplemented with protease inhibitors and phosphatase inhibitors (Roche). Following clarification of cell lysates by centrifugation, protein levels were quantified with the BCA protein assay (Thermo Fisher Scientific). Ten micrograms of whole cell lysate and five micrograms of cell fractionation lysate were resolved by SDS-PAGE in 7.5% or 15% polyacrylamide gels depending on the molecular weight of the proteins to be analyzed. Gels were electrotransferred into nitrocellulose membranes (BioRad) and protein transfer was verified by Amido Black staining before immunoblotting. Proteins were detected with antibodies against p63(Abcam ab5309, 1/4000 dilution), MYC (Cell Signaling Technology 9402, diluted 1/1,000), and FGFR3 (Abcam ab133644, diluted 1/5,000). Alpha-tubulin and beta-actin (Sigma Aldrich references T6199 and A2228, respectively; both diluted at 1/20,000) were used as loading controls. The

secondary antibodies used were HRP-linked anti-mouse IgG and anti-rabbit IgG (Cell Signaling Technology references 7076 and 7074, respectively, both diluted at 1/3,000).

For shTP63i cells, cells were plated in 60mm plates and treated with or without dox for 72 hours. Protein was then extracted using RIPA-EDTA and protease cocktail inhibitor. Protein concentration was measured using the Bradford method (MERK1103060500). Proteins (50-80uG) were resolved in polyacrylamide gels and then transferred to PVDF membranes and incubated with antibodies against p63 (ab53039) b-Actin (sigma A5441) MT1-MMP (sc-30074) and reveled using Li-cor C-Digit Blot scanner. Images were analyzed by Gel Pro Analyzer software.

Human samples

We used RNA extracted from 163 bladder tumors of our Carte d'Identites cohort (CIT; 79 NMIBCs and 80 MIBCs). Tumor samples were flash-frozen and stored at -80°C immediately after transurethral resection or cystectomy. Immunohistochemical analysis by hematoxylin and eosin (H&E) staining confirmed that all tumor samples contained more than 80% of tumor cells (staining of sections adjacent to the samples used for transcriptome analyses).All patients provided informed consent, and the study was approved by the institutional review boards of the Foch, Institut Gustave Roussy and Henri Mondor Hospitals. Extraction of RNA, DNA and protein from the surgical samples was done by cesium chloride density centrifugation as previously described[64]. FGFR3 mutations were determined through the SNaPshot technique.

Transcriptomic data was further obtained from 98 NMIBC and 97 MIBC tumors using the Affymetrix Human Exon 1.0 ST array. Differential gene expression analysis was done with the LIMMA R package, and *P*-values were adjusted for multiple testing through the Benjamini-Hochberg (FDR) method.

RNA-seq

For a whole genome profiling experiment, MGH-U3 cells were transfected for 48 hours with TP63 siRNA #11 (as described above)

Triplicate RNA isolates from siTP63 transfected and control (lipofectamine RNA iMax, Invitrogen) were prepared using the Qiagen RNA easy minikit supplemented with DNase treatment, and RNA sample quality was controled with the Agilent 2100 Bioanalyzer system.RNA sequencing was carried out on stranded mRNA (1 µg) with an Illumina NovaSeq S1 sequencing system at a sequencing depth of 30 million reads per sample. Quality control and filtering of data was carried out using FastQC (Babraham Bioinformatics Institute, Cambridge). Filtered reads were mapped to the hg19 human genome and

annotated using the STAR aligner. Statistically significant differences in gene expression were determined by performing a LIMMA-VOOM using eBayes statistics. The P-values were adjusted for multiple testing through the Benjamini-Hochberg (FDR) method.

P63-ChIP-seq

MGH-U3 cells were cross-linked in 1% formaldehyde for 10min at room temperature. The reaction was stopped with glycine (final concentration 125mM, 5min incubation at room temperature). Fixed cells were then washed twice with PBS and harvested with a cell scraper. Following centrifugation (11500rpm 5min); the cell pellet was resuspended in extraction buffer (250mM sucrose, 10mL Tris-HCl pH8, 10mM $MgCl_2$, 1% Triton and 5mM β-mercaptoethanol) supplemented with protease inhibitors (Roche). Cells were centrifuged at 3,000g for 10min and recovered samples were analyzed using the ChIP-IT High Sensitivity kit (Active Motif, 53040). ChIP was carried out using a p63 antibody (Cell Signaling Technology, D2K8X XP, 13109). Sequencing and analysis of results was carried out in collaboration with the sequencing platform of the IGBMC Strasbourg. Sequences were aligned to the human hg19 genome using Bowtie[65] and peaks were called using the SPP v1.14 R package from the Kundaje Lab Tools[66]. ChIP-seq data was processed following the ENCODE-DCC ChIP-seq pipeline 2 (Anshul Kundaje, https://github.com/ENCODE-DCC/chip-seq-pipeline2). ChIP-seq results represent two independent experiments.

P63 Gene targets in MGH-U3

Genes being directly regulated by p63 in MGH-U3 cells were determined as those genes that had a statistically significant change of expression following the knockdown of *TP63* (|logFC|>1 ; adjusted *P*-value ≤0.05) and additionally presented a strong peak at +/- 5kb from their TSS (P63-ChIP-seq). Amongst these genes, those having a statistically significant logFC≤1 would be considered as p63 activated targets, whereas those having a logFC≥1 would be considered as p63 repressed targets.

Gene ontology enrichment

The DAVID Functional Annotation Tool v6.8 was used to identify biological processes (GO-BPs) that were enriched in the set of p63 target genes (n=330 activated targets, n=391 repressed targets). Significantly enriched GO-BPs were considered as those having an adjusted *P*-value (Benjamini-Hochberg) ≤0.05.

Spheroid growth

3D cell cultures were generated by the hanging drop seeding method 3x103 cells in 20ul of complete medium, during 72hs (MGHU3) or 96hs (UM-UC-14) and then plated on agar

coated-96 wells plates. Cultured medium with or without DOX was completely replaced twice a week and images were taken weekly. Diameter was measured using Image J software and then surface was calculated. After 30 days, spheroids were fixed in methacarn and embedded in paraffin to be sliced and immunostained using a standard immunofluoresce method. p63 was stained with primary antibody CM163B (Biocare medical) and secondary antibody Alexa 488 (ab150113). Nuclei were stained using DAPI (Cas28718-90-3, Sigma-Aldrich).

Gelatin degradation assay

FITC-labeled gelatin was obtained from Invitrogen. Coverslips coated with fluorescent gelatin were prepared as described by Artym et al. 2006. In brief, coverslips (18-mm diameter) were coated with polilysin 0.5 µg/ml for 20 min at room temperature, washed with PBS, and fixed with 0.5% glutaraldehyde (Sigma-Aldrich) for 15 min. After three washes, the coverslips were inverted on an 80-µl drop of 0.2% fluorescently labeled gelatin and incubated for 10 min at room temperature. After washing with PBS, coverslips were incubated in 5 mg/ml sodium borohydride for 3 min, washed three times in PBS, and finally incubated in 2 ml of complete medium for a minimum of 2 h before adding the cells. Cells were treated with or without DOX (100 ng/ml) for 72 hours before the assay and plated on coated coverslips in DMEMF12 containing 10% FCS. Then, cells were incubated at 37°C for 5 hours (MGHU3) or overnight (UM-UC-14). Cells were fixed with PFA 4% for 20 min. Cells were inmunostained for F-actin (AA22283, Life technologies) and nuclei with DAPI (Cas28718-90-3, Sigma-Aldrich) and imaged with 40× objective in at least 15 fields per experiment. For quantification of degradation, the total area of degraded matrix in one field (black pixels) measured using the Image J was divided by the total number of phalloidin-labeled cells in the field to define a degradation index.

Wound healing assay

Cells were seeded in 6 wells plates and treated with or without DOX during 72h. Two wounds were performed in each well and then a PBS wash was performed to eliminate the released cells. Culture medium was replaced for 2% FBS medium. Pictures were taken immediately (t0) and 24 hours later (t1). Wound area was measured in both situations using Image J and migrated area was calculated using the formula: (At1*100)/At0 and then relativized to control.

In vivo models

i. Mice UPII-hFGFR3-S249C transcriptome

We used the transcriptome from tumor samples of a previously established FGFR3-induced murine model of bladder tumors [Moreno-Vega, Shi, Fontugne, Meng 2019 unpublished]. In brief, the expression of the human FGFR3IIIb carrying the S249C mutation was specifically targeted to the urothelium of mice through the use of the murine uroplakin II promoter. Mice developed hyperplastic lesions and low-grade papillary tumors from 6 and 18 months of age respectively. Genes exhibiting a change of expression between UPII-hFGFR3 mice tumors and control urothelium were defined via the analysis of extracted mRNA using the Affymetrix Mouse Exon 1.0 ST array, followed by the use of the LIMMA algorithm to define statistically significant changes of expression. The *P*-values were adjusted for multiple testing through the Benjamini-Hochberg (FDR) method [Moreno-Vega, Shi, Fontugne, Meng 2019 unpublished].

ii.FGFR3 inhibition in vivo (PDX model)

Protein lysates (20µg) derived from previously established patient-derived bladder cancer xenografts (PDX) of mice treated or not with the pan-FGFR inhibitor BGJ398 (30mg/kg/day; 4 days) were used for immunoblotting[20].

iii. Nude mice tumor growth

Nude male mice were obtained from: CNEA (Comisión Nacional de Energía Atómica). All the procedures were approved by the CICUAL (Comité Institucional para el Uso y Cuidado de Animales de Laboratorio) Instituto de Oncología A.H. Roffo (Protocol number 2017/03)
Human bladder cancer TP63 silenced cells were injected subcutaneously in the right flank of 20 mice (2x106 cells in 100ul of PBS). When the tumors were palpable (1mmx1mm) 10 mice received 1g/L of DOX in the drinking water (DOX group) and 10 mice only water (Ctrl group). Tumors were measured using caliper twice a week and volume was calculated with the formula: 3/4π x (largest diameter) x (shorter diameter)2. At the end of the experiment mice were sacrificed and tumors removed, fixed in methacarn and latter paraffin embedded to be sliced and immunostained. p63 was labeled with the primary antibody CM163B (Biocare medical) and secondary antibody Alexa 546(A110003). PCNA with primary antibody (2586, Cell Signalling) and secondary Alexa 488 (ab150113). Nuclei were stained using DAPI (Cas28718-90-3, Sigma-Aldrich).

Statistical analysis

All experiments were independently carried out two or three times, with each experiment presenting triplicates. Data are presented as means ±SD. Wilcoxon's unpaired tests were used for multiple comparisons. For microarray data analysis, the linear models for microarray data (LIMMA)[67] R package was used and *P*-values were adjusted via the Benjamini-Hochberg method.

Author contributions statement

Conceptualization, M.E., F.R, C.L., I.B.P.; *Methodology*, A.M.V., J.P., M.Z., C.G.; *Investigation*, A.M.V., M.Z. J.P, F.D, F.D., M.S, C.B, M.L; *Formal Analysis*, A.M.V., M.Z, F.D, C.G, M.S, L.D.; *Writing –Original Draft*, A.M.V., C.L, I.B.P.; *Writing –Review & Editing*, all the authors; *Visualization,* A.M.V., M.Z, M.S; *Funding Acquisition*, M.E, C.L, I.B.P. and F.R; *Resources*, T.L, Y.A, P.L, A.M.E, L.D.; *Data curation*, E.C.; *Supervision*, C.L, I.B.P. and F.R.;

References

1. Babjuk, M. *et al.* European Association of Urology Guidelines on Non-muscle-invasive Bladder Cancer (TaT1 and Carcinoma In Situ) - 2019 Update. *European Urology* **76**, 639–657 (2019).
2. Gierth, M. & Burger, M. Bladder cancer: Progress in defining progression in NMIBC. *Nat. Rev. Urol.* **10**, 684–685 (2013).
3. Funt, S. A. & Rosenberg, J. E. Cancer and Future Horizons. **14**, 221–234 (2018).
4. Park, J. C., Citrin, D. E., Agarwal, P. K. & Apolo, A. B. Multimodal management of muscle-invasive bladder cancer. *Curr. Probl. Cancer* **38**, 80–108 (2014).
5. Collin, M.-P. *et al.* Discovery of Rogaratinib (BAY 1163877): a pan-FGFR Inhibitor. *ChemMedChem* **13**, 437–445 (2018).
6. Loriot, Y. *et al.* Erdafitinib in Locally Advanced or Metastatic Urothelial Carcinoma. *N. Engl. J. Med.* **381**, 338–348 (2019).
7. Pal, S. K. *et al.* Efficacy of BGJ398, a Fibroblast Growth Factor Receptor 1–3 Inhibitor, in Patients with Previously Treated Advanced Urothelial Carcinoma with *FGFR3* Alterations. *Cancer Discov.* **8**, 812–821 (2018).
8. Siefker-Radtke, A. O. A phase 2 study of JNJ-42756493, a pan-FGFR tyrosine kinase inhibitor, in patients (pts) with metastatic or unresectable urothelial cancer (UC) harboring FGFR gene alterations. *J. Clin. Oncol.* (2016).
9. Hedegaard, J. *et al.* Comprehensive Transcriptional Analysis of Early-Stage Urothelial Carcinoma. *Cancer Cell* **30**, 27–42 (2016).
10. Robertson, A. G. *et al.* Comprehensive Molecular Characterization of Muscle-Invasive Bladder Cancer. *Cell* **171**, 540-556.e25 (2017).
11. Robertson, A. G. *et al.* Comprehensive Molecular Characterization of Muscle-Invasive Bladder Cancer. *Cell* **171**, 540-556.e25 (2017).
12. Shi, M. J. *et al.* APOBEC-mediated Mutagenesis as a Likely Cause of FGFR3 S249C Mutation Over-representation in Bladder Cancer. *Eur. Urol.* **76**, 9–13 (2019).
13. Tomlinson, D., Baldo, O., Harnden, P. & Knowles, M. FGFR3 protein expression and its relationship to mutation status and prognostic variables in bladder cancer. *J. Pathol.* **213**, 91–98 (2007).
14. Chell, V. *et al.* Tumour cell responses to new fibroblast growth factor receptor tyrosine kinase inhibitors and identification of a gatekeeper mutation in FGFR3 as a mechanism of acquired resistance. *Oncogene* **32**, 3059–3070 (2013).
15. Flaherty, K. T. *et al.* Combined BRAF and MEK Inhibition in Melanoma with BRAF V600 Mutations. *N. Engl. J. Med.* **367**, 1694–1703 (2012).
16. Pearson, A. *et al.* Parallel RNA Interference Screens Identify EGFR Activation as an Escape Mechanism in FGFR3-Mutant Cancer. *Cancer Discov.* **3**, 1058–1071 (2013).
17. Niederst, M. J. & Engelman, J. A. Bypass mechanisms of resistance to receptor tyrosine kinase

inhibition in lung cancer. *Science Signaling* **6**, (2013).
18. Wang, J. *et al.* Ligand-associated ERBB2/3 activation confers acquired resistance to FGFR inhibition in FGFR3-dependent cancer cells. *Oncogene* **34**, 2167–2177 (2015).
19. Wang, L. *et al.* A Functional Genetic Screen Identifies the Phosphoinositide 3-kinase Pathway as a Determinant of Resistance to Fibroblast Growth Factor Receptor Inhibitors in FGFR Mutant Urothelial Cell Carcinoma [Figure presented]. *Eur. Urol.* **71**, 858–862 (2017).
20. Mahe, M. *et al.* An FGFR3/MYC positive feedback loop provides new opportunities for targeted therapies in bladder cancers. *EMBO Mol. Med.* e8163 (2018). doi:10.15252/emmm.201708163
21. Linde, J., Schulze, S., Henkel, S. G. & Guthke, R. Data- and knowledge-based modeling of gene regulatory networks: An update. *EXCLI J.* **14**, 346–378 (2015).
22. Elati, M. *et al.* LICORN: Learning cooperative regulation networks from gene expression data. *Bioinformatics* **23**, 2407–2414 (2007).
23. Emmert-Streib, F., Glazko, G. V., Altay, G. & Simoes, R. de M. Statistical inference and reverse engineering of gene regulatory networks from observational expression data. *Frontiers in Genetics* **3**, (2012).
24. Huynh-Thu, V. A., Irrthum, A., Wehenkel, L. & Geurts, P. Inferring regulatory networks from expression data using tree-based methods. *PLoS One* **5**, (2010).
25. Margolin, A. A. *et al.* ARACNE: An algorithm for the reconstruction of gene regulatory networks in a mammalian cellular context. *BMC Bioinformatics* **7**, (2006).
26. Chebil, I., Nicolle, R., Santini, G., Rouveirol, C. & Elati, M. Hybrid method inference for the construction of cooperative regulatory network in human. *IEEE Trans. Nanobioscience* **13**, 97–103 (2014).
27. Nicolle, R., Radvanyi, F. & Elati, M. CoRegNet: Reconstruction and integrated analysis of co-regulatory networks. *Bioinformatics* **31**, 3066–3068 (2014).
28. Meyers, R. M. *et al.* Computational correction of copy number effect improves specificity of CRISPR-Cas9 essentiality screens in cancer cells. *Nat. Genet.* **49**, 1779–1784 (2017).
29. Palmbos, P. L. *et al.* ATDC/TRIM29 drives invasive bladder cancer formation through miRNA-mediated and epigenetic mechanisms. *Cancer Res.* **75**, 5155–5166 (2015).
30. Trabelsi, N., Setti Boubaker, N., Said, R. & Ouerhani, S. Notch Pathway: Bioinformatic Analysis of Related Transcription Factors within Bladder Cancer Types and Subtypes. *IRBM* **39**, 261–267 (2018).
31. Warrick, J. I. *et al.* FOXA1, GATA3 and PPARIγ Cooperate to drive luminal subtype in bladder cancer: A molecular analysis of established human cell lines. *Sci. Rep.* **6**, (2016).
32. Zhang, X. *et al.* Somatic Superenhancer Duplications and Hotspot Mutations Lead to Oncogenic Activation of the KLF5 Transcription Factor. *Cancer Discov.* **8**, 108–125 (2018).
33. Choi, W. *et al.* Identification of distinct basal and luminal subtypes of muscle-invasive bladder cancer with different sensitivities to frontline chemotherapy. *Cancer Cell* **25**, 152–65 (2014).
34. Guo, C. C. *et al.* Dysregulation of EMT Drives the Progression to Clinically Aggressive Sarcomatoid Bladder Cancer. *Cell Rep.* **27**, 1781-1793.e4 (2019).
35. Karni-Schmidt, O. *et al.* Distinct expression profiles of p63 variants during urothelial development and bladder cancer progression. *Am. J. Pathol.* **178**, 1350–1360 (2011).
36. Castro-Castro, A. *et al.* Cellular and Molecular Mechanisms of MT1-MMP-Dependent Cancer Cell Invasion. *Annu. Rev. Cell Dev. Biol.* **32**, 555–576 (2016).
37. Lodillinsky, C. *et al.* p63/MT1-MMP axis is required for in situ to invasive transition in basal-like breast cancer. *Oncogene* **35**, 344–357 (2016).
38. Hernández, S. *et al.* Prospective study of FGFR3 mutations as a prognostic factor in nonmuscle invasive urothelial bladder carcinomas. *J. Clin. Oncol.* **24**, 3664–3671 (2006).
39. Bradner, J. E., Hnisz, D. & Young, R. A. Transcriptional Addiction in Cancer. *Cell* **168**, 629–643 (2017).
40. Lee, T. I. & Young, R. A. Transcriptional regulation and its misregulation in disease. *Cell* **152**, 1237–1251 (2013).
41. Kamoun, A. *et al.* A Consensus Molecular Classification of Muscle-invasive Bladder Cancer. *Eur. Urol.* (2019). doi:10.1016/j.eururo.2019.09.006
42. Rebouissou, S. *et al.* EGFR as a potential therapeutic target for a subset of muscle-invasive bladder cancers presenting a basal-like phenotype. *Sci. Transl. Med.* **6**, 244ra91 (2014).
43. Choi, W. *et al.* p63 expression defines a lethal subset of muscle-invasive bladder cancers. *PLoS One* **7**, (2012).
44. He, Y. *et al.* Impaired delta Np63 expression is associated with poor tumor development in transitional cell carcinoma of the bladder. *J. Korean Med. Sci.* **23**, 825–832 (2008).
45. Gaya, J. M. *et al.* Δnp63 expression is a protective factor of progression in clinical high grade

T1 bladder cancer. *J. Urol.* **193**, 1144–1150 (2015).
46. Koga, F. *et al.* Impaired ΔNp63 expression associates with reduced β-catenin and aggressive phenotypes of urothelial neoplasms. *Br. J. Cancer* **88**, 740–747 (2003).
47. Fukushima, H. *et al.* Loss of ΔNp63α promotes invasion of urothelial carcinomas via N-cadherin/Src homology and collagen/extracellular signal-regulated kinase pathway. *Cancer Res.* **69**, 9263–9270 (2009).
48. Papadimitriou, M. A. *et al.* ΔNp63 transcript loss in bladder cancer constitutes an independent molecular predictor of TaT1 patients post-treatment relapse and progression. *J. Cancer Res. Clin. Oncol.* **145**, 3075–3087 (2019).
49. Park, B. J. *et al.* Frequent alteration of p63 expression in human primary bladder carcinomas. *Cancer Res.* **60**, 3370–4 (2000).
50. Chen, Y. *et al.* A double dealing tale of p63: an oncogene or a tumor suppressor. *Cellular and Molecular Life Sciences* **75**, 965–973 (2018).
51. Tran, M. N. *et al.* The p63 protein isoform ΔNp63α inhibits epithelial-mesenchymal transition in human bladder cancer cells: Role of miR-205. *J. Biol. Chem.* **288**, 3275–3288 (2013).
52. Barretina, J. *et al.* The Cancer Cell Line Encyclopedia enables predictive modelling of anticancer drug sensitivity. *Nature* **483**, 603–607 (2012).
53. Delpuech, O. *et al.* Identification of pharmacodynamic transcript biomarkers in response to FGFR inhibition by AZD4547. *Mol. Cancer Ther.* **15**, 2802–2813 (2016).
54. Lambert, S. A. *et al.* The Human Transcription Factors. *Cell* **172**, 650–665 (2018).
55. Schmeier, S., Alam, T., Essack, M. & Bajic, V. B. TcoF-DB v2: Update of the database of human and mouse transcription co-factors and transcription factor interactions. *Nucleic Acids Res.* **45**, D145–D150 (2017).
56. Schaefer, M. H. *et al.* Hippie: Integrating protein interaction networks with experiment based quality scores. *PLoS One* **7**, (2012).
57. Franceschini, A. *et al.* STRING v9.1: Protein-protein interaction networks, with increased coverage and integration. *Nucleic Acids Res.* **41**, (2013).
58. Keshava Prasad, T. S. *et al.* Human Protein Reference Database - 2009 update. *Nucleic Acids Res.* **37**, (2009).
59. Kou, Y. *et al.* ChEA2: Gene-set libraries from ChIP-X experiments to decode the transcription regulome. in *Lecture Notes in Computer Science (including subseries Lecture Notes in Artificial Intelligence and Lecture Notes in Bioinformatics)* **8127 LNCS**, 416–430 (2013).
60. Kulakovskiy, I. V. *et al.* HOCOMOCO: Expansion and enhancement of the collection of transcription factor binding sites models. *Nucleic Acids Res.* **44**, D116–D125 (2016).
61. Marbach, D. *et al.* Tissue-specific regulatory circuits reveal variable modular perturbations across complex diseases. *Nat. Methods* **13**, 366–370 (2016).
62. Jiang, C., Xuan, Z., Zhao, F. & Zhang, M. Q. TRED: A transcriptional regulatory element database, new entries and other development. *Nucleic Acids Res.* **35**, (2007).
63. Shannon, P. *et al.* Cytoscape: A software Environment for integrated models of biomolecular interaction networks. *Genome Res.* **13**, 2498–2504 (2003).
64. Calderaro, J. *et al.* PI3K/AKT pathway activation in bladder carcinogenesis. *Int. J. Cancer* **134**, 1776–1784 (2014).
65. Langmead, B. Aligning short sequencing reads with Bowtie. *Curr. Protoc. Bioinforma.* (2010). doi:10.1002/0471250953.bi1107s32
66. Landt, S. G. *et al.* ChIP-seq guidelines and practices of the ENCODE and modENCODE consortia. *Genome Research* **22**, 1813–1831 (2012).
67. Ritchie, M. E. *et al.* Limma powers differential expression analyses for RNA-sequencing and microarray studies. *Nucleic Acids Res.* **43**, e47 (2015).

Supplementary Figures

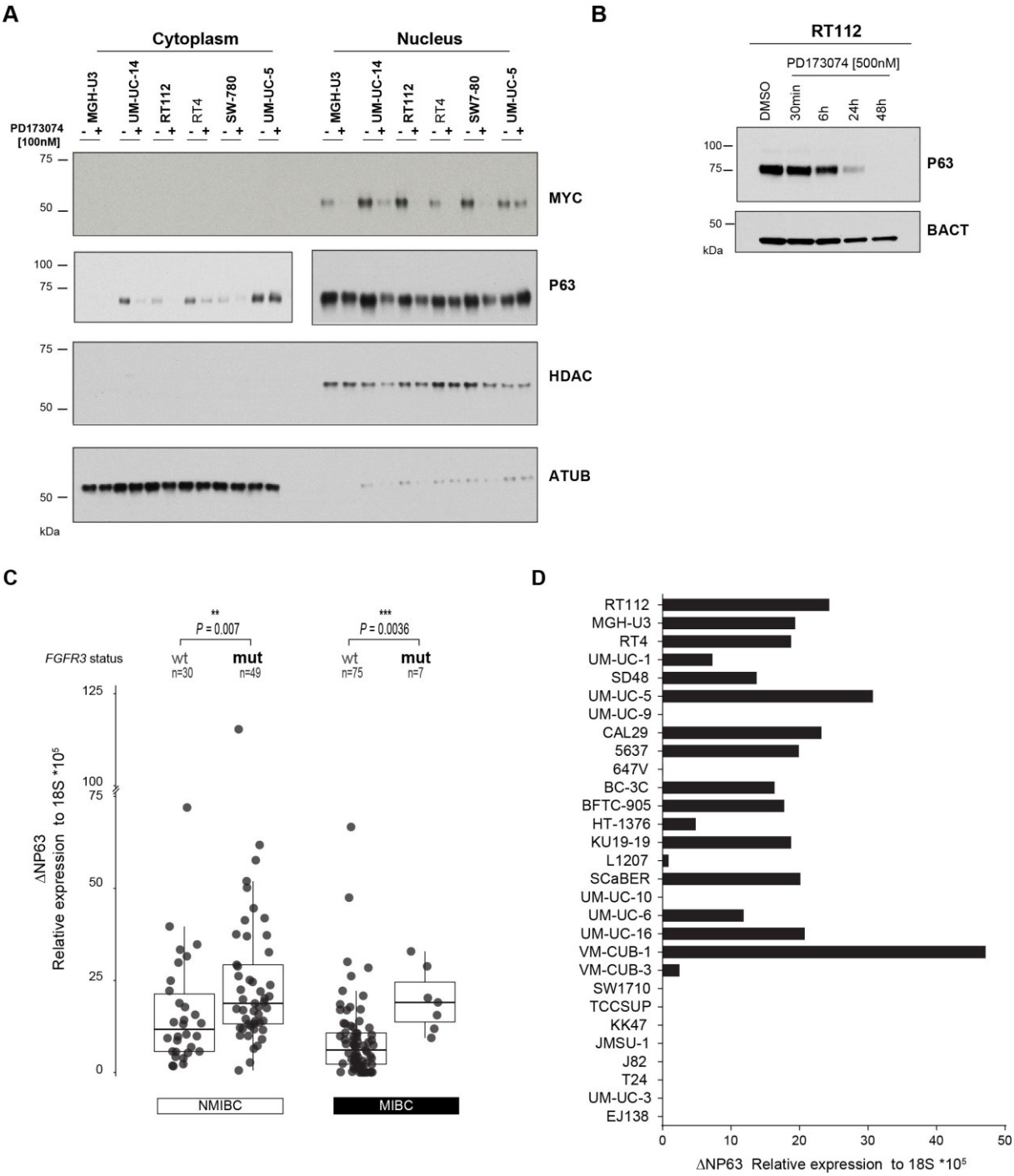

Supp Figure 1. TP63 expression in bladder cancer cell lines and human bladder tumors harboring an altered-*FGFR3*.

A. Western blot assay comparing p63 expression levels at the cytoplasmic and nuclear compartments of FGFR3-dependent cells (MGH-U3, UM-UC-14, RT112, RT4, SW780) treated or not with a pan-FGFR inhibitor (PD173074, 100nM, 40h). UM-UC-5 cells expressing a wt*FGFR3* were used as control. MYC protein levels were used as a technical control based on the previously reported FGFR3-MYC regulatory-loop[20]. Proteins used as loading control and control of cell fraction purity were: HDAC and ATUB.

B. RT112 cells were treated with DMSO (48hours) or the pan-FGFR inhibitor PD173074 [500nM] for 30min, 6h, 24, and 48h. Cell lysates were recovered at each time point and analyzed by immunoblotting using antibodies against p63. Actin was used as a loading control.

C. Relative expression of the ΔNp63 isoform with respect to the 18S ribosomal subunit in human bladder tumors from the CIT cohort (NMIBC; *n* = 79, MIBC *n* = 82).

D. Relative expression of the ΔNp63 isoform with respect to the 18S ribosomal subunit in bladder cancer derived cell lines.

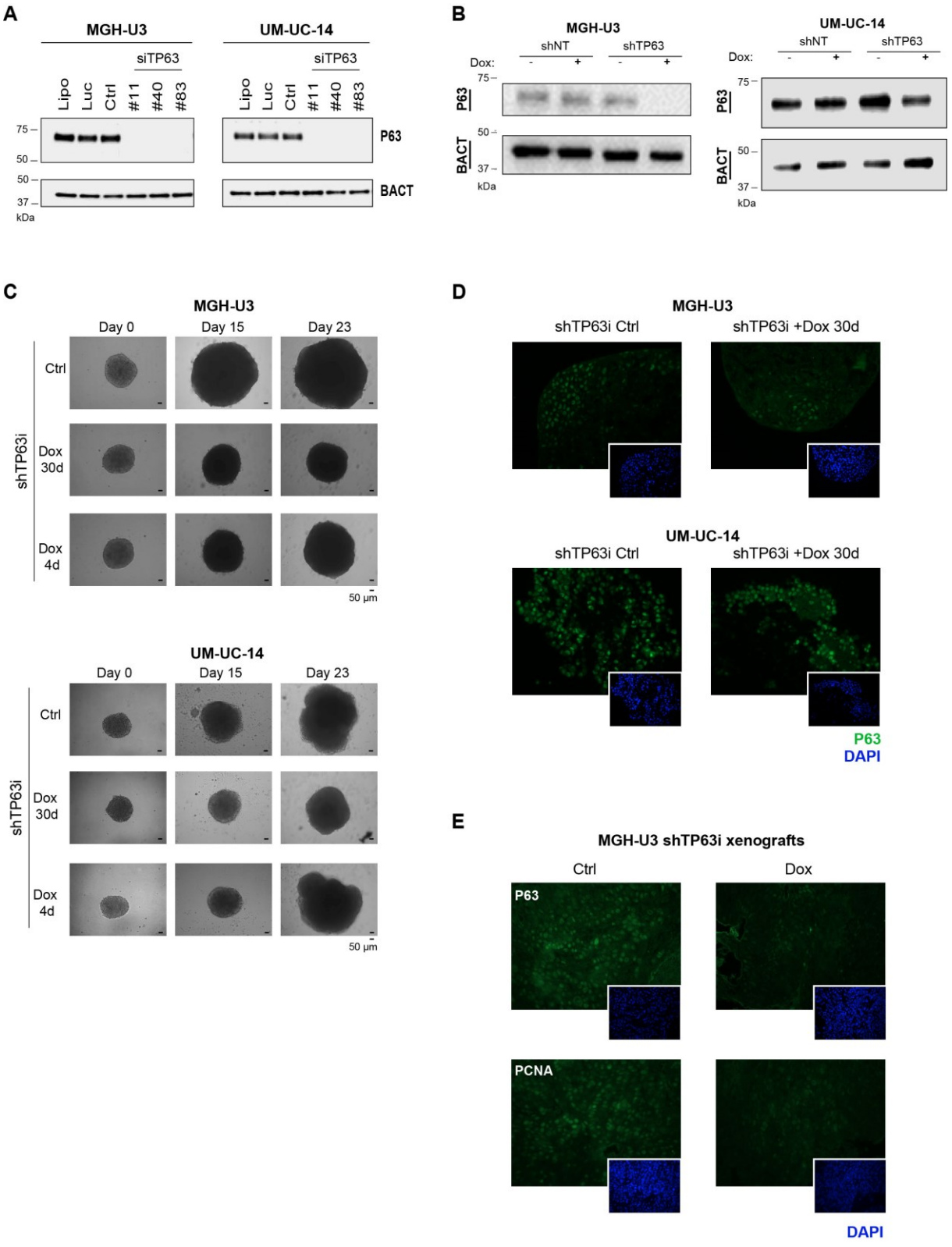

Supp Figure 2. Transient and stable knockdown of *TP63* in FGFR3-mutated bladder cancer cell lines.

A. MGH-U3 and UM-UC-14 were transfected with three different siRNAs targeting *TP63* (siTP63 #11, #40, #83). Forty-eight hours after transfection, cell lysates were recovered and analyzed by immunoblotting with antibodies against p63. Actin (BACT) was used as a loading control.

B. MGH-U3 and UM-UC-14 cells stably expressing a doxycycline (Dox)-inducible shRNA directed against *TP63* (shTP63i) were treated or not with Dox and efficiency of knockdown was corroborated by western blotting of p63. Actin (BACT) was used as a loading control.

C. Representative microscopy images of MGH-U3 shTP63i#4 and UM-UC-14 shTP63i#4 treated or not with Dox for a long (30 days; 30d) or short (4 days; 4d) time period. Scale bar represents 50μm.

D-E. Representative immunofluorescence images of p63 staining-cells in: D. MGH-U3 shTP63i#4 and UM-UC-14 shTP63i#4 cultures treated or not with Dox and E. Tumors from xenografted mice generated with MGH-U3 shTP63i#4 cells, and treated or not with Dox for 30 days.

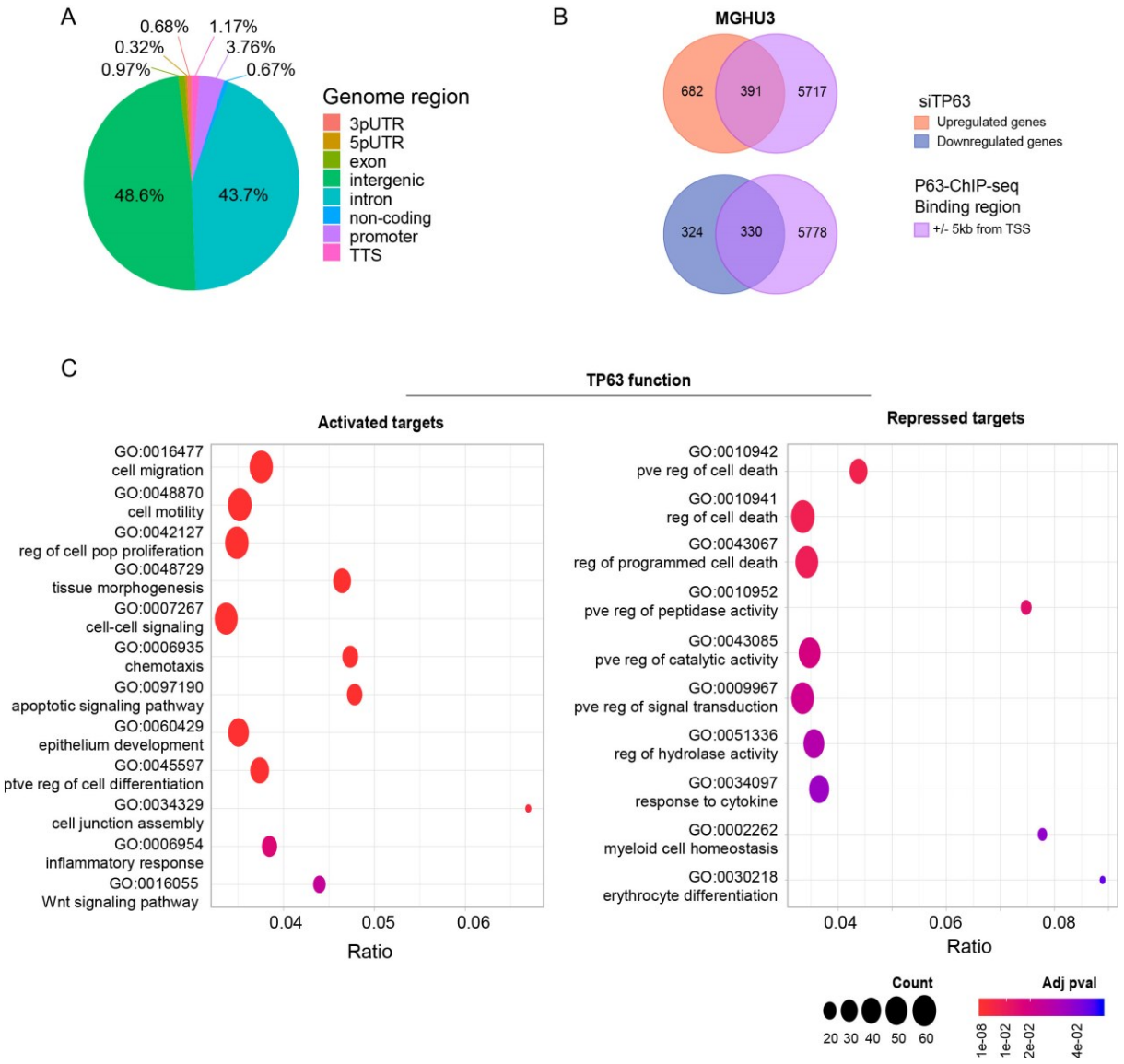

Supp Figure 3. P63 target genes in an altered-FGFR3 bladder cancer context.

A. Genome binding profile of p63 from P63-ChIPseq of MGH-U3 cells.

B. Selection of possible p63 targets in MGH-U 3 cells through a Venn Diagram analysis of significant P63ChIPseq peaks (+/- 5kb from the transcription start site; TSS) and genes whose expression was significantly changed upon knockdown of *TP63* in MGH-U3. Results represent two independent experiments.

C. Significantly enriched Gene Ontology Biological Processes (GO/BPs) of the p63 targets determined in Supp Figure 3B. Only GO/BPs presenting an adjusted p-value <0.05 with at least 10 genes contributing to their enrichment were considered. P-values were adjusted by the Benjamini-Hochberg method.